Simultaneous Microfocus Raman and Microfocus XRD: Probing the Deformation of a Single High-Performance Fiber

Richard J. Davies,* Manfred Burghammer, and Christian Riekel

European Synchrotron Radiation Facility, 6 Rue Jules Horowitz, BP220, Grenoble Cedex 9, France

Received January 11, 2006; Revised Manuscript Received May 5, 2006

ABSTRACT: Combined microfocus Raman and microfocus XRD is employed to probe the in situ deformation of a single poly(*p*-phenylene terephthalamide), PPTA, or Kevlar fiber. The experimental results are obtained from the same point on the sample simultaneously, using coaxial microfocus X-ray and laser beams. The 1610 cm^{-1} Raman band shifts linearly to a lower wavenumber with macroscopic stress, while the crystal lattice along the fiber axis direction extends linearly. The resulting Raman band shift rate and crystal modulus are -3.3 cm^{-1}/GPa and 214 GPa, respectively. Raman band broadening with increasing stress suggests an increasing stress heterogeneity between the crystalline and amorphous fractions. Meanwhile, meridional layer line narrowing is interpreted as a deformation-induced homogenization of the PPTA fiber's skin-core structure. These results demonstrate the benefits of combining experimental techniques in situ which offer complementary phase and volume selectivity. In this case, macroscopic fiber deformation can be qualitatively explained using low- and high-stress uniform-strain mechanical models. At low stresses, linear Raman band broadening with stress can be attributed to a phase-related difference in mechanical properties. At high stresses, an increasing degree of crystalline domain orientation causes heterogeneous stiffening within the PPTA fiber structure. Consequently, the amorphous fraction remains "understressed" during subsequent deformation.

1. Introduction

Raman spectroscopy and X-ray diffraction (XRD) have become independently established as important techniques for studying structure−property relationships in high-performance polymer fibers. This is because both techniques are able to monitor micromechanical parameters during macroscopic deformation, without the need for sample sectioning. Stress transfer can therefore be traced between the different hierarchical levels within a material. By understanding this relationship between macroscopic and microscopic stress, the structural origins of specific mechanical properties can be determined. When studying fiber deformation, the use of a single fiber rather than a bundle offers several advantages. These include a more accurate determination of local stress, the elimination of averaging between different fibers in the bundle, and mechanical data that are comparable to standard tensile testing results. Both Raman spectroscopy and XRD can collect data from single fibers using microfocus techniques.[1,2] Microfocus Raman spectroscopy (μRaman) can be performed using a number of commercial systems. In the most common configuration, an optical microscope is used to obtain a high-flux, small-diameter beam for illuminating small samples.[2] In contrast, microfocus X-ray diffraction (μXRD) requires the high brilliance and low divergence of a synchrotron radiation (SR) source.[1] The need for dedicated microfocus optics and sensitive detectors confines μXRD to specialist beamlines at large SR facilities.[1]

The information provided by Raman spectroscopy and XRD is complementary on many levels. For example, they probe microscopic material structure over different length scales, from individual molecular bonds to large-scale domains. They also differ in the information they provide on different phases within a single material (e.g., amorphous and crystalline) and can be used to select complementary sampling volumes due to their different penetration depths within one material. As a result, several studies have successfully investigated materials using both techniques in sequential experiments.[3−6] In many cases this is straightforward as the same specimen can be used for both tests. However, this is precluded for deformation studies due to their destructive nature. For these investigations multiple specimens are required, and the resulting variability tends to dominate experimental error. High-performance fibers are especially susceptible to such errors as they frequently exhibit a large standard deviation in diameter, both between different individual fibers and along a single fiber's length.[7] Such heterogeneities can result in different experimental results over a relatively short axial distance.[8] To overcome this, experiments combining multiple techniques can be carried out simultaneously, with both data sets collected from the same point on the fiber. The technical challenge of performing a combined μXRD/μRaman experiment is considerable. Both sets of microfocusing optics, apertures, and detectors must be integrated so as not to restrict beam delivery and data collection. Thus, while several studies have combined macroscopic XRD and Raman spectroscopy in situ,[9−11] the coupling of μXRD and μRaman has only become available recently.[12] This study reports on the first combined μXRD and μRaman investigation of a single high-performance fiber during deformation. The two techniques are used to study the evolution of microscopic stress during macroscopic deformation.

2. Experimental Section

2.1. Materials. Single poly(*p*-phenylene terephthalamide) (or PPTA) fibers of the Kevlar*49* variety are characterized in this study. Kevlar is a high-performance polymeric fiber with a strength and modulus reported as 2.8 GPa and 123 GPa, respectively.[4] The fiber's mechanical properties can be attributed to a well-oriented, highly crystalline structure of extended polymeric chains within a sheetlike hydrogen-bonded network.[13,14] This promotes a high degree of three-dimensional crystallinity, which in turn provides mechanical stability in both tension and compression. For this reason, PPTA is a popular choice for composite applications where compressive

* Corresponding author. E-mail: rdavies@esrf.fr.

10.1021/ma0600658 CCC: $33.50
Published on Web 06/14/2006

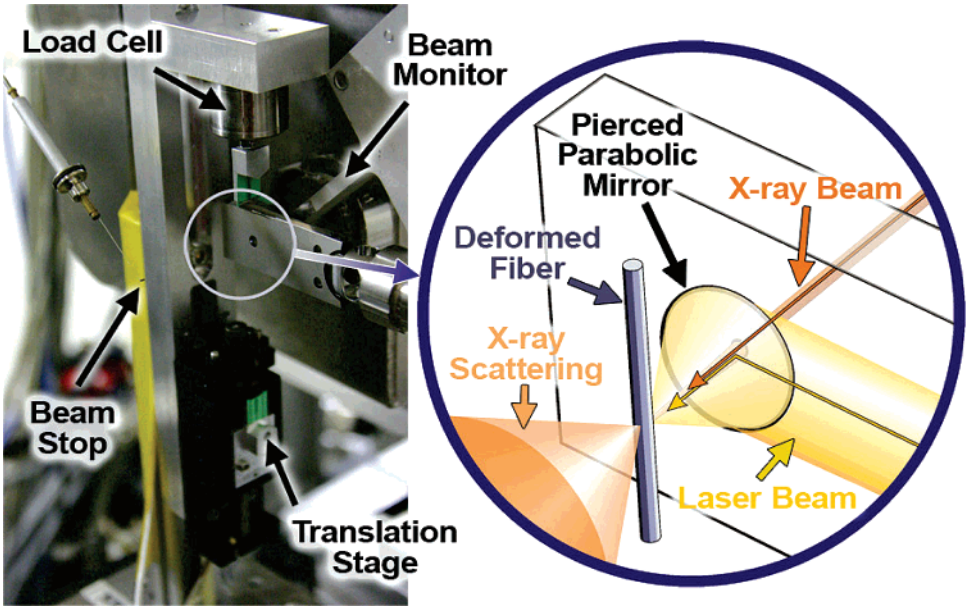

Figure 1. (left) Annotated photograph of the deformation rig and μRaman probe in situ on the beamline and (right) a schematic showing probe geometry and integration in detail.

properties are a critical selection criterion. The polymeric chain repeat of PPTA is shown below:

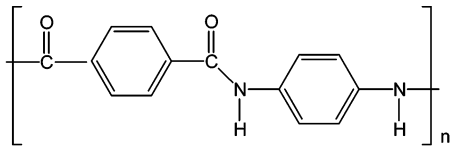

Polymeric repeat unit of the PPTA molecular backbone

2.2. Simultaneous μRaman and μXRD. Simultaneous μRaman and μXRD was performed at the microfocus beamline ID13 of the European Synchrotron Radiation Facility.[1] The beamline was configured with a pair of short focal-length Kirkpatrick-Baez (KB) mirrors, giving an X-ray beam diameter of ~1 μm at the focal position. Diffraction patterns were collected using a 16 bit MARCCD 165 area detector (pixel size of ~80 μm), with a sample-to-detector distance of 123 mm. In situ μRaman was carried out using a custom-built system, designed and constructed by Renishaw PLC, in collaboration with the ID13 beamline.[12] The base system consists of a Renishaw InVia spectrometer, configured with a 500 mW near-IR 785 nm diode laser, holographic Raleigh rejection filters and a 1200 lines/mm grating. To achieve simultaneous on-axis data collection, the system uses a μRaman probe, mounted between the final X-ray guard aperture (incorporating a beam monitor) and the sample position. The probe is coupled to the spectrometer with a single-mode fiber optic to minimize spatial requirements around the sample environment. A pierced parabolic mirror located within the probe-head focuses the laser beam onto the sample, while allowing the X-ray beam to pass through freely. At the focal position, the laser spot size is ~1 μm in diameter, similar to the dimensions of the focused X-ray beam.[12] The μRaman probe is aligned (using a motorized translation stage) so that the focal positions of both beams coincide. The alignment procedure is simplified by the ability to visualize the laser spot on the sample surface using an integrated camera and white-light illumination incorporated into the probe. This provides a means of verifying that the sample is positioned at the common focal position and, with the aid of a suitable calibration object, verifying that the two beams coincide. An electrical pulse from the beamline control system allows the μRaman and μXRD data to be collected simultaneously. This trigger is used to open both the X-ray and laser shutters as well as activating the respective detectors. Thus, the two beams are delivered coaxially to the same position on the sample at the same time. The fact that both CCDs have similar readout times ensures that the cycle time for successive collections is compatible between the two systems. A common exposure time of 5 s was used for both techniques (carried out in the 16-bunch storage ring operation mode).

2.3. In Situ Deformation. To deform single fibers in situ, a long gauge-length deformation rig was used. When attached to the beamline sample positioning stage, the mounted fiber can be positioned at the common focal position of the X-ray and laser beams. The rig consists of a remotely controlled linear translation stage. This is used to apply tension to the fiber while a load cell and transducer indicator allow the resulting force to be recorded. This information can then be used to calculate macroscopic fiber stress. Deformation was carried out using a 50 mm gauge length, with a minimal force applied to the fiber prior to the start of the experiment (to stabilize the undeformed fiber). μRaman and μXRD data were collected at incremental load levels until fiber failure occurred. Figure 1 shows a photograph of the single fiber deformation rig, as mounted on the beamline positioning stage, and a schematic showing the data collection geometry and system components featuring in the photograph.

2.4. Data Treatment. μXRD data treatment was carried out using a combination of the Fit2D software application[15] and specialist software for batch-fitting scattering intensity profiles.[16] Prior to analysis, all diffraction data were background subtracted to reduce the influence of air scattering. To determine radial reflection positions, the diffraction patterns were azimuthally integrated to generate scattering profiles of each reflection of interest. These were then fitted using either Lorentzian or Pseudo-Voigt functions to determine peak positions and widths. To determine lattice strain along the fiber axis (longitudinal crystal strain), a modified Bragg equation was used. Further details of this calculation are provided elsewhere.[3] To calculate orientation parameter, the equatorial reflections were radially integrated over a 180° range, around each radial reflection maxima. The resulting azimuthal profiles were then used for the calculation of orientation parameter (f_c) according to the method followed by Riekel et al. for single PPTA fibers.[17] All of the μXRD results presented within this study are averaged from both hemispheres of each diffraction pattern. The analysis of Raman spectra was performed using the WiRE 2.0 software application. Raman bands within the selected spectral ranges were batch-fitted using specialist functions combining weighted Lorentzian and Gaussian contributions. Where quoted, errors are calculated from fitting certainty with confidence bands at 95% shown for linear fits.

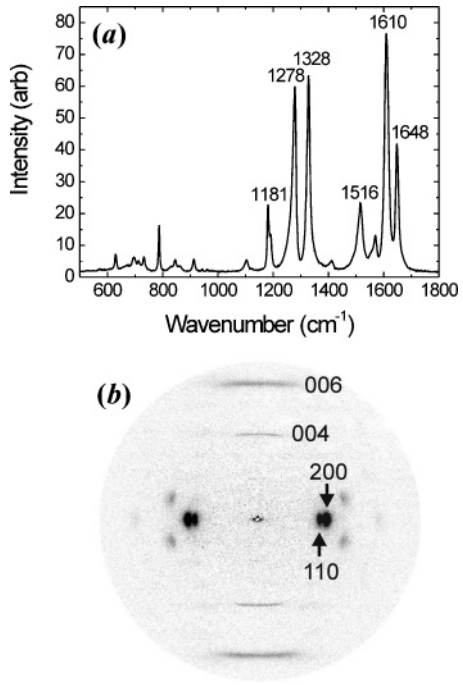

Figure 2. (a) Extended Raman spectrum and (b) indexed diffraction pattern obtained from a single undeformed PPTA fiber (collected simultaneously).

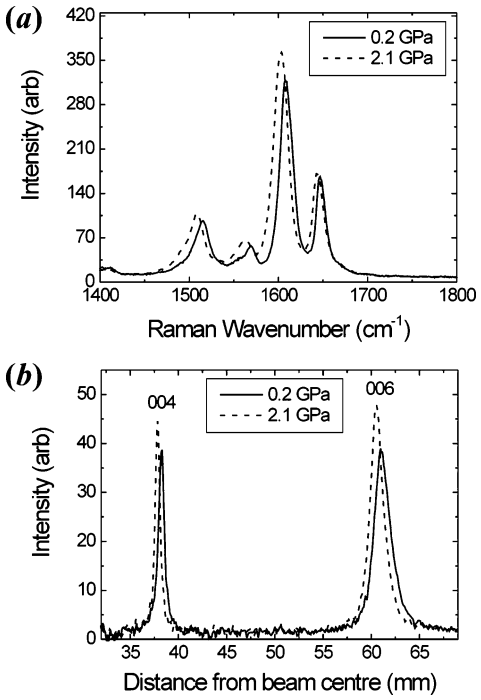

Figure 3. Influence of macroscopic fiber stress on (a) the 1610 cm^{-1} Raman band and (b) meridional layer line scattering from a single PPTA fiber.

3. Results

3.1. Undeformed Fiber Characterization. Figure 2 shows an extended Raman spectrum, and a diffraction pattern, collected from of a single PPTA fiber. The Raman spectrum is annotated with the wavenumber positions of the major PPTA Raman bands while the diffraction pattern has been indexed according to the PPTA unit cell.[13,14] Both data sets were collected simultaneously from the unstrained fiber, prior to deformation. In Figure 2a there are several strong Raman bands within the range 1100−1700 cm^{-1}. The band positions are in good agreement with previous studies of the PPTA fiber type.[4,8] The most intense and frequently studied band at 1610 cm^{-1} can be assigned to the vibrational mode 8a of the *p*-phenylene ring.[4,18]

The diffraction pattern shown in Figure 2b is characterized by strong meridional and equatorial scattering, indicative of a high degree of crystallinity. The azimuthally narrow angular range of the equatorial reflections indicates a high degree of crystalline domain alignment along the fiber axis direction. The off-axis reflections suggest extensive three-dimensional order within the crystalline regions. This is not observed for other high-performance fibers such as poly(*p*-phenylene benzobisoxazole) (or PBO) as they lack the hydrogen-bonded structure of the PPTA fiber type.[3] From the reflection positions in Figure 2b, the unit cell dimensions can be calculated on the basis of the published monoclinic structure (where $\gamma = 90°$).[13,14] This yields values of $a = 7.78$ Å, $b = 5.19$ Å, and $c = 12.9$ Å. These are in agreement with the unit cell dimensions obtained in a number of previous studies.[14,19−21]

3.2. Single Fiber Deformation. Figure 3 shows the influence of macroscopic fiber stress on the positions of the 1610 cm^{-1} Raman band and meridional wide-angle X-ray scattering (WAXS) reflections. The Raman band and meridional reflections shift with increasing stress, both of which are well-documented phenomena. The stress-induced band shift shown in Figure 3a can be attributed to changes in bond length and force constants, resulting in a shift of the vibrational mode.[8,22] For tension, this is measured as a band shift to a lower wavenumber.[8,22] For the 1610 cm^{-1} Raman band shown in Figure 3a, this indicates direct stretching of the *p*-phenylene ring within PPTA molecules.[4,18] The simultaneous increase in band intensity may originate from a slight difference in the position of the fiber with respect to the laser focal position. The fact that this phenomenon does not feature in previous studies of the PPTA fiber type supports this possibility.[4,23] There is no clear evidence in Figure 3a of Raman band asymmetry during deformation, as observed for the high-performance fiber poly(*p*-phenylene benzobisthiazole) (or PBT).[7] This indicates that the molecules do not become "overstressed" during deformation.

The stress-induced changes in meridional "layer line" position shown in Figure 3b can be attributed to a dimensional change of the crystal lattice. The meridional reflections are associated with electron density periodicities along the fiber axis of the unit cell (*c*-axis), equivalent to the chain direction for PPTA. A shift of the meridional reflections toward the beam center indicates an increase in this unit cell dimension, which corresponds to a positive strain on the crystal lattice. Thus, while the Raman results represent the deformation of individual molecular bonds, the X-ray results represent the deformation of a molecular array.

As well as a shift in the meridional "layer line" position, a radial narrowing also occurs with increasing stress. This is consistent between both the 004 and 006 "layer lines", decreasing from a full width at half-maximum (fwhm) of 0.77° at 0 GPa to 0.56° at 2.5 GPa for the 006 reflection (values are in 2θ°). Any variation in the position of the fiber between measurements can be excluded as the integrated intensity remains consistent (to within 5%), and the X-ray beam divergence is relatively low (<1 mrad). While a change in crystallite size could also be responsible, a previous study reports no evidence for stress-induced crystallization in high-performance fibers.[24] Furthermore, the degree of radial narrowing in this case is well beyond the elastic deformation limit of a PPTA crystal, as it would correspond to a 25% increase in mean crystal

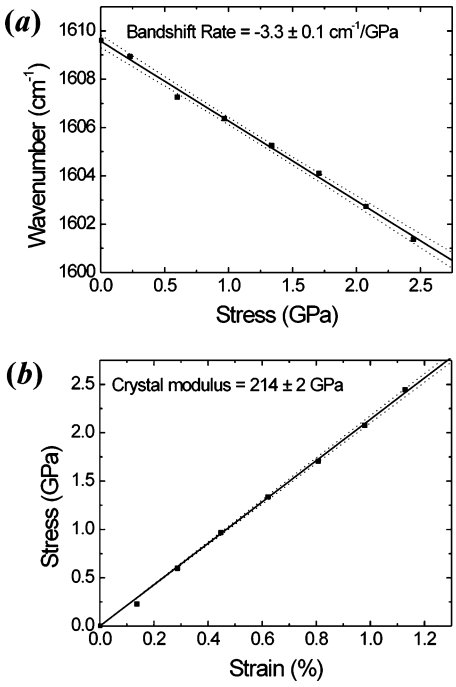

Figure 4. Determination of (a) stress-induced Raman band shift rate of the 1610 cm^{-1} band and (b) crystal modulus calculated from the 004 and 006 meridional reflections.

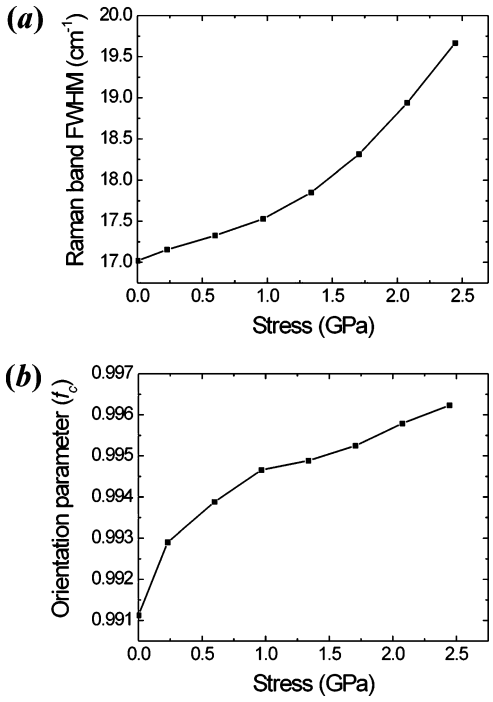

Figure 5. Influence of applied macroscopic stress on (a) the width of the 1610 cm^{-1} Raman band and (b) the degree of axial crystalline domain orientation.

size. Therefore, this result indicates that increasing macroscopic stress decreases the variation in stress between crystalline domains.

It is interesting to note that a study of the PBO fiber type reports the opposite behavior as that observed in this study for PPTA.[24] Thus, in the case of PBO, deformation results in broader "layer lines", interpreted as an increasingly heterogeneous stress distribution.[24] A possible explanation for this difference could be the lack of hydrogen bonds between PBO molecules which could allow for greater molecular independence. However, it is difficult to see how this could extend to crystalline domain level while still maintaining three-dimensional order. An alternative explanation could be the use of fiber bundles in the PBO study.[24] This could result in the measured variation reflecting different stresses between individual fibers within the bundle rather than individual domains within a single fiber.

3.3. Raman Band Shift and Crystal Modulus. Figure 4 shows the relationship between the position of the 1610 cm^{-1} Raman band and longitudinal (axial) crystal strain, both with respect to applied macroscopic stress. The Raman band shift shown in Figure 4a is linear, in good agreement with previous studies for aromatic high-modulus fibers.[3,4] This demonstrates that applied macroscopic fiber stress is directly proportional to the microscopic stress on individual molecules. This direct relationship highlights molecular-scale contributions to macroscopic mechanical properties. It also explains why the Raman band shift parameter is useful as a calibration tool to calculate local fiber stresses within composite materials.[25] The linear fit in Figure 4a gives the rate of stress-induced band shift as -3.3 ± 0.1 cm^{-1}/GPa. This is lower than the universal band shift rate of -4 cm^{-1}/GPa obtained for a number of aromatic high-modulus fibers, including Kevlar.[4,26] However, the observation of a stress-induced Raman band shift rate of less than -4 cm^{-1}/GPa is not confined to this study. For example Kitagawa et al. observe values for PBO ranging from -2.93 to -3.57 cm^{-1}/GPa for different fiber varieties.[27,28] The fact that these are well below the -4 cm^{-1}/GPa model value is explained in terms of plastic deformation or a large skin-core variation.[28]

Figure 4b shows the variation of crystal stain with increasing fiber stress. Crystal strain is calculated from the change in the *c*-axis of the crystal lattice, averaged from the 004 and 006 meridional reflections (for both hemispheres). The relationship between crystal strain and macroscopic fiber stress is linear. This demonstrates that microscopic lattice strain is directly proportional to macroscopic fiber stress and therefore also proportional to *p*-phenylene ring stretching. From the linear fit in Figure 4b, the crystal modulus of 214 ± 2 GPa is in good agreement with previous experimental observations of 200 GPa.[29,30] This is also close to the calculated value of 182 GPa[29] and extrapolated estimates of 190−200 GPa.[4,31] The fact that the crystal modulus is in agreement with previous studies suggests the calculation of macroscopic stress in this study is accurate. Thus, despite the Raman band shift rate being lower than the model value of -4 cm^{-1}/GPa, it is also likely to be accurate.

3.4. Raman Band Broadening and Crystalline Domain Orientation. Figure 5 shows the relationship between the width of the 1610 cm^{-1} Raman band, crystalline domain orientation, and applied macroscopic stress. In Figure 5a, the Raman band broadens with increasing stress, as reported previously for the PBO and PPTA fiber types.[4,27,28] This band broadening phenomenon can be attributed to a variation in local stresses between molecules which translates directly into a distribution in Raman band position. The results in Figure 5a therefore correspond to an increasing stress heterogeneity with increasing macroscopic stress. Below 1.0 GPa, the Raman band broadens linearly with applied stress. However, above this value, the band broadening rate increases. This nonlinearity above 1.0 GPa is direct evidence of a stress-induced change occurring in the fiber structure.

Figure 5b shows the change in the degree of axial crystalline domain orientation with increasing deformation. The degree of orientation is expressed in terms of the f_c parameter, calculated

from azimuthal broadening of the 110 and 200 equatorial reflections.[17] The azimuthal profiles were fitted using Lorentzian functions, where the values shown in Figure 5b represent an average obtained from both diffraction pattern hemispheres. A detailed account of the calculation method and the required assumption of rotational symmetry about the fiber axis are provided elsewhere.[17] The initial and final orientation parameter values (f_c) of 0.991 (0 GPa) and 0.996 (2.5 GPa) compare favorably with a previous study which reports values of 0.990 (0 GPa) and 0.994 (2.5 GPa).[17] The small (but consistent) difference might be attributed to skin-core variations in the PPTA fiber type. Whereas the values quoted in this study are from single diffraction patterns from the centre of the fiber, the previous study reports an average of several measurements across the entire fiber diameter.[17] Any variations due to the fitting procedure are negligible (the average f_c error is $<7.0 \times 10^{-5}$ for a fitting uncertainty of $\pm 0.03°$). It is interesting to note that the relationship between the orientation parameter and macroscopic fiber stress is nonlinear at low stresses but almost linear at high stresses. This transition occurs at a fiber stress of ~1.0 GPa, which corresponds to the Raman band broadening transition in Figure 5a.

3.5. A Structural Interpretation of Experimental Results. Until this point, the experimental results obtained using Raman spectroscopy and XRD have only been discussed individually and in rather general terms. However, by considering the structural origins of the results in more detail, the fiber's internal structure can be indirectly probed. This is possible because of the complementary nature of the information provided by the two techniques, offering a means of separating the different contributions toward the fiber's bulk mechanical properties. This complementary aspect can be demonstrated by comparing Raman band broadening and meridional layer line narrowing behavior during macroscopic fiber deformation. While the former indicates an increasing stress heterogeneity between molecules, the latter indicates an increasing stress homogeneity between crystalline domains. This result, which initially seems conflicting, can be explained by the experimental techniques' different phase sensitivities. Raman spectroscopy probes all molecules within the sampling volume while the WAXS results are exclusive to the crystalline phase. It is therefore quite possible for the two techniques to generate results featuring opposing trends. In doing so, this demonstrates that Raman band broadening can be associated with a phase-related variation which is invisible to WAXS. This explanation of Raman band broadening forms the basis of several existing models.[6,32,33]

The Raman results provide a measure of the variation in stress between the different phases. However, this does not explain the origin of meridional layer line narrowing with increasing macroscopic stress. This increasing stress homogeneity between the crystalline domains implies an intraphase factor must also be considered in addition to any interphase difference. One possibility is a decrease in radial anisotropy during fiber deformation. PPTA fibers are known to exhibit a radially anisotropic skin-core morphology.[34,35] The difference between crystalline domain orientation in the fiber skin and core regions is also known to decrease with increasing macroscopic stress.[36] It therefore seems logical to extend this to an accompanied reduction in the local stress distribution between those regions. On this basis, radial narrowing of meridional reflections can be interpreted as the deformation-induced homogenization of this skin-core fiber morphology. The limited depth-penetration of Raman spectroscopy in opaque polymers such as PPTA may explain why this trend is not apparent in Raman band broadening behavior. Alternatively, it may simply indicate that interphase variations mask any weaker intraphase contribution in the Raman spectra. Whichever the case, the two techniques suggest that macroscopic fiber stress increases the microscopic stress heterogeneity between the crystalline and amorphous fractions, while at the same time reducing any skin-core variations in stress.

To further explain the structural origins of Raman band broadening in PPTA, it is necessary to consider a mechanical model to account for individual contributions. While many complex models have been developed, only a straightforward bicomponent model is needed to qualitatively describe PPTA micromechanics. At this basic level models tend to assume either uniform stress or uniform strain to account for the behavior of the crystalline and noncrystalline elements. For example, a bicomponent, uniform-stress model can be used to explain and calculate Raman band broadening behavior.[32,33] Although this type of model has been employed successfully for the high-performance fiber PBO,[32] it requires an assumption that there is no band shift within the amorphous fraction.[32] For this reason, this type of model is difficult to justify when all molecules within the fiber are required to be under the same stress. In addition, it also implies the generation of considerable strain disparities between the crystalline and noncrystalline regions (due to their difference in modulus). It is difficult to see how this can be physically accommodated, especially in a fiber such as PPTA, which has a high shear modulus due to its hydrogen-bonded network. As an alternative, a uniform-strain (parallel) model can account for Raman band broadening in terms of different stresses within the crystalline and noncrystalline regions (for the same strain). Prasad and Grubb use a variation of this model to explain band broadening in high-modulus polyethylene (PE) fibers.[6] Their model describes deformation in terms of different mechanisms becoming dominant at different stress levels and therefore incorporates nonlinearity.[6] At low stresses, all PE chains are stressed in the same way and so Raman band broadening is linear.[6] However, at high stresses, the noncrystalline chains and taut tie molecules are stressed more than the crystals, resulting in significant nonlinearity.[6] While this model is reasonable for PE, it cannot be directly translated to PPTA deformation. For example, in PE both crystal strain and Raman band shifts become nonlinear at high stresses, in contrast with the linear relationships observed for PPTA.

Of the two basic model types, a uniform-strain model seems more reasonable for PPTA, primarily because it is structurally more agreeable. Clearly, the fact that tensile strain is greater than longitudinal crystal strain indicates that it is an oversimplification, but it is nevertheless sufficient for this discussion. In addition, the nonlinear Raman band broadening in Figure 5a supports a distinction between different stresses. This would correspond to the changing dominance of deformation mechanisms, as successfully employed in the PE model of Prasad and Grubb.[6] In the case of PPTA, the changes occurring at a macroscopic fiber stress of 1.0 GPa appear to mark a transition point. Thus, the deformation micromechanics of PPTA can be qualitatively described in terms of low- and high-stress uniform-strain models.

3.5.1. A Low-Stress Uniform-Strain PPTA Model. At low stresses, and assuming uniform strain, linear band broadening can be readily explained by the difference in the mechanical modulus of the crystalline and noncrystalline fractions. The fact that a material's modulus varies between different crystallographic phases is widely accepted and frequently exploited during polymer processing. Indeed, phase-related modulus

variations have been demonstrated experimentally for PPTA fibers by mechanical testing.[37] On this basis, uniform strain will result in a stress difference between the stiff crystalline (and mesophase) component and the more extensible noncrystalline component. This translates into different band shift rates between the different fractions, which manifests itself as the observed broadening effect during macroscopic deformation.

The WAXS results in Figure 5b show that macroscopic fiber stress increases the degree of crystalline domain orientation with respect to the fiber axis. This can be attributed to a high shear-stress component acting upon crystalline domains, resulting in their rotation. The orientation increase is greatest during the initial stages of deformation, when shear forces are maximized and there are fewer physical constraints. Such stress-induced changes are well-known in high-performance fibers.[17,36,38] Indeed, crystalline domain orientation is an important parameter in dictating their mechanical properties. Nevertheless, the fact that there is linear Raman band broadening with applied stress during the initial stages of deformation indicates that local stresses remain proportional between the different phases. Thus, macroscopic stress is transferred directly through the hierarchical structure of the fiber resulting in proportional local stresses on crystallographic and molecular length scales throughout the fiber.

3.5.2. A High-Stress Uniform-Strain PPTA Model. At high stresses, and assuming uniform strain, nonlinear Raman band broadening can be explained by a heterogeneous stiffening within the fiber structure. This can be considered as a change in the relative stiffness between the crystalline and noncrystalline phases. This phase-specific change in the Raman band shift rate causes band broadening nonlinearity during subsequent deformation. Critically, the transition to nonlinear Raman band broadening at 1.0 GPa coincides with a change in the relationship between crystalline domain orientation and macroscopic stress. This implies that heterogeneous stiffening is linked to the measured orientation improvement within the crystalline fraction. In terms of crystalline domain orientation, this transition point reflects a number of combined effects. As domains become increasingly oriented the shear stress component is reduced, while rotational freedom also becomes limited (such as due to chain entanglements). These factors, coupled with the high degree of crystalline domain orientation, result in an orientation-related stiffening of the crystalline fraction. This may correspond to strain hardening, which has been reported during deformation of the Kevlar fiber type.[4,39] This is observed as an increase in fiber modulus due to the nonreversible alignment of molecular chains to the fiber axis.[4,39]

In the case of PPTA, the missing link between heterogeneous stiffening and nonlinear Raman band broadening is provided by the XRD results. The fact that crystal strain remains proportional to macroscopic fiber stress indicates that stiffening of the crystalline fraction increases the bulk mechanical modulus of the fiber. This is perhaps unsurprising considering that the crystalline and mesophase fraction is reported to account for 70% of the fiber bulk.[40] With the fiber's bulk modulus increase related exclusively to the crystalline phase, and assuming uniform strain, the noncrystalline component will be "understressed" during further deformation. In other words, for a given macroscopic stress, the noncrystalline fraction will extend less at high stresses as it is constrained by the stiffer crystalline component. This is therefore opposite to Prasad and Grubb's PE model where the noncrystalline regions are "overstressed". This explains why band broadening is nonlinear for PPTA while crystal strain remains linear, unlike for PE.

One possible criticism of the proposed high-stress model is the linear relationship observed between macroscopic fiber stress and Raman band shift in Figure 4a. However, this may simply reflect the small fraction of noncrystalline material within the fiber structure. With a crystalline and mesophase fraction of 70%,[40] it is conceivable that the 1610 cm^{-1} Raman band's function fit is biased. Thus, the Raman band position is predominantly influenced by the crystalline phase and therefore shifts linearly in response to macroscopic fiber stress. This may also explain the lack of band asymmetry in Figure 3a, which is expected with heterogeneous stiffening. In this case the relatively small noncrystalline fraction, coupled with the close proximity between the 1610 and 1648 cm^{-1} Raman bands, masks any obvious asymmetry.

4. Conclusions

μRaman and μXRD have been combined successfully to probe in situ deformation of single PPTA fibers. The results show that such experiments are technically possible, despite the complicated delivery system required to obtain coincidental, coaxial, and simultaneous X-ray and laser beams with similar micron-scale dimensions. For PPTA, a Raman band shift rate of -3.3 cm^{-1}/GPa is observed, which is lower than the universal value of -4 cm^{-1}/GPa, reported for other aromatic polymers.[4] However, the crystal modulus of 214 GPa is in good agreement with previous studies, suggesting that the macroscopic stress values used to calculate Raman band shift are accurate. Simultaneous Raman band broadening and meridional layer line narrowing with macroscopic stress can be explained through the different phase and volume sensitivities of the two techniques. Thus, macroscopic fiber stress increases the microscopic stress heterogeneity between the crystalline and amorphous fractions, while at the same time reducing any skin-core variations in stress.

The experimental results obtained using Raman spectroscopy and XRD can be qualitatively interpreted through the application of low- and high-stress uniform-strain mechanical models. At low stresses, the degree of crystalline domain orientation increases; however, there is no relative change between crystalline and noncrystalline mechanical properties. Thus, macroscopic stress is transferred directly through the hierarchical structure of the fiber resulting in proportional local stresses on crystallographic and molecular length scales throughout the fiber. At high stresses, the fiber structure stiffens heterogeneously due to the increasing orientation of crystalline domains to the fiber axis. As the crystalline and mesophase fractions constitute the majority of the fiber's structure, this increases the mechanical modulus. Consequently, further deformation leads to the minority amorphous fraction being "understressed", observed as nonlinear Raman band broadening with stress.

This study demonstrates several advantages offered by the simultaneous collection of μRaman and μXRD data. For example, the experimental results obtained in this study are immediately comparable, allowing direct correlations to be made and providing a means of verifying specific parameters, such as Raman band shift rates. The coupling of these complementary techniques provides additional insight into material micromechanics and structure, with the added advantage that all experimental data are collected together, reducing experimental time.

Acknowledgment. The authors acknowledge Renishaw PLC for their contribution toward the design, development, and installation of the μRaman apparatus.

CDV

References and Notes

(1) Riekel, C.; Davies, R. J. *Curr. Opin. Colloid Interface Sci.* **2005**, *9*, 396.
(2) Meier, R. J.; Kip, B. J. *Microbeam Anal. (San Francisco)* **1994**, *3*, 61.
(3) Davies, R. J.; Montes-Moran, M. A.; Riekel, C.; Young, R. J. *J. Mater. Sci.* **2001**, *36*, 3079.
(4) Yeh, W.-Y.; Young, R. J. *Polymer* **1999**, *40*, 857.
(5) Moonen, J. A. H. M.; Roovers, W. A. C.; Meier, R. J.; Kip, B. J. *J. Polym. Sci., Part B* **1992**, *30*, 361.
(6) Prasad, K.; Grubb, D. T. *J. Polym. Sci., Part B* **1989**, *27*, 381.
(7) Day, R. J.; Robinson, I. M.; Zakikhani, M.; Young, R. J. *Polymer* **1987**, *28*, 1833.
(8) Young, R. J. *J. Text. Inst.* **1995**, *86*, 361.
(9) Bryant, G. K.; Gleeson, H. F.; Ryan, A. J.; Fairclough, J. P. A.; Bogg, D.; Goossens, J. G. P.; Bras, W. *Rev. Sci. Instrum.* **1998**, *69*, 2114.
(10) Bras, W.; Ryan, A. J. *J. Mol. Struct.* **1996**, *383*, 309.
(11) Ran, S.; Fang, D.; Sics, I.; Toki, S.; Hsiao, B. S.; Chu, B. *Rev. Sci. Instrum.* **2003**, *74*, 3087.
(12) Davies, R. J.; Burghammer, M.; Riekel, C. *Appl. Phys. Lett.* **2005**, *87*, 264105.
(13) Gardner, K. H.; English, A. D.; Forsyth, V. T. *Macromolecules* **2004**, *37*, 9654.
(14) Lui, J.; Cheng, S. Z. D.; Geil, P. H. *Polymer* **1996**, *37*, 1413.
(15) Hammersley, A. P. ESRF Internal Report ESRF97HA02T, 1997.
(16) Davies, R. J. *J. Appl. Crystallogr.* **2006**, *39*, 262.
(17) Riekel, C.; Dieing, T.; Engstrom, P.; Vincze, L.; Martin, C.; Mahendrasingam, A. *Macromolecules* **1999**, *32*, 7859.
(18) Kim, P. K.; Chang, C.; Hsu, S. L. *Polymer* **1986**, *27*, 34.
(19) Nakamae, K.; Nishino, T.; Airu, X. *Polymer* **1992**, *33*, 4898.
(20) Northolt, M. G. *Eur. Polym. J.* **1974**, *10*, 799.
(21) Tashiro, K.; Kobayashi, M.; Tadokoro, H. *Macromolecules* **1977**, *10*, 413.
(22) Tashiro, K. *Prog. Polym. Sci.* **1993**, *18*, 377.
(23) Young, R. J.; Ang, P. P. *Polymer* **1992**, *33*, 975.
(24) Kitagawa, T.; Yabuki, K. *J. Polym. Sci., Part B* **2000**, *38*, 2937.
(25) Andrews, M. C.; Young, R. J. *J. Raman Spectrosc.* **1993**, *24*, 539.
(26) Sirichaisit, J.; Young, R. J. *Polymer* **1999**, *40*, 3421.
(27) Kitagawa, T.; Tashiro, K.; Yabuki, K. *J. Polym. Sci., Part B* **2002**, *40*, 1269.
(28) Kitagawa, T.; Yabuki, K.; Young, R. J. *J. Macromol. Sci., Phys.* **2002**, *41*, 61.
(29) Tashiro, K.; Kobayashi, M. *Polymer* **1991**, *32*, 454.
(30) Gaymans, R. J.; Tijssen, J.; Harkema, S.; Bantjes, A. *Polymer* **1976**, *17*, 517.
(31) Li, T.; Tashiro, K.; Kobayashi, M.; Tadokoro, H. *Macromolecules* **1987**, *20*, 347.
(32) Kitagawa, T.; Tashiro, K.; Yabuki, K. *J. Polym. Sci., Part B* **2002**, *40*, 1281.
(33) Tashiro, K.; Wu, G.; Kobayashi, M. *Polymer* **1988**, *29*, 1769.
(34) Panar, M.; Avakian, P.; Blume, R. C.; Gardner, K. H.; Gierke, T. D.; Hang, H. H. *J. Polym. Sci., Polym. Phys. Ed.* **1983**, *21*, 1955.
(35) Li, L.-S.; Allard, L. F.; Bigelow, W. C. *J. Macromol. Sci., Phys.* **1983**, *2*, 269.
(36) Davies, R. J.; Montes-Moran, M. A.; Riekel, C.; Young, R. *J. J. Mater. Sci.* **2003**, *38*, 2105.
(37) Graham, J. F.; McCague, C.; Warren, O. L.; Norton, P. R. *Polym. Commun.* **2000**, *41*, 4761.
(38) Kitagawa, T.; Yabuki, K. *J. Polym. Sci., Part B* **2000**, *38*, 2901.
(39) Northolt, M. G. *Polymer* **1980**, *21*, 1199.
(40) Ran, S.; Fang, D.; Zong, X.; Hsiao, B. S.; Chu, B.; Cunniff, P. M. *Polymer* **2001**, *42*, 1601.

MA0600658